Structure of a Protein Photocycle Intermediate by Millisecond Time-Resolved Crystallography

Ulrich K. Genick *et al.*

Science **275**, 1471 (1997);
DOI: 10.1126/science.275.5305.1471

Science (print ISSN 0036-8075; online ISSN 1095-9203) is published weekly, except the last week in December, by the American Association for the Advancement of Science, 1200 New York Avenue NW, Washington, DC 20005.

2. W. C. Merrick and J. W. B. Hershey, in *Translational Control*, J. W. B. Hershey, M. B. Mathews, N. Sonenberg, Eds. (Cold Spring Harbor Laboratory Press, Cold Spring Harbor, NY, 1996), pp. 31–69.
3. A. Pause and N. Sonenberg, *Curr. Opin. Struct. Biol.* **3**, 953 (1993).
4. F. Rozen *et al.*, *Mol. Cell. Biol.* **10**, 1134 (1990).
5. F. V. Fuller-Pace, *Trends Cell Biol.* **4**, 271 (1994).
6. K. Struhl and R. W. Davis, *J. Mol. Biol.* **136**, 309 (1980); K. Struhl, *Nucleic Acids Res*. **13**, 8587 (1985).
7. D. J. Jamieson, B. Rahe, J. Pringle, J. D. Beggs, *Nature* **349**, 715 (1991).
8. V. Thuillier, S. Stettler, A. Sentenac, P. Thuriaux, M. Werner, *EMBO J.* **14**, 351 (1995).
9. A 2.9-kb Xho I–Sal I DNA fragment containing the complete *DED1* gene (*6*) was subcloned into pRS315 (*CEN/LEU2*) to yield pDED1009 and incubated with hydroxylamine [R. S. Sikorski and J. D. Boeke, *Methods Enzymol.* **194**, 302 (1991)]. The mutagenized DNA was amplified and transformed into yeast strain YTC75 [MAT**a** *ded1::TRP1 ura3-52 lys2-801 ade2-101 trp1-Δ1 his3-Δ200 leu2-Δ1* pDED1008 (*DED1/CEN/URA3*)]. Transformants on leucine-dropout plates were replica-plated onto 5-fluoroorotic acid (5-FOA) plates to identify conditional mutants that failed to grow at either 37° or 15°C. Linkage between the growth phenotype and the mutated *ded1* allele was verified by recloning the *ded1* insert and repeating the plasmid shuffling. Mutations in the *ded1* alleles were identified by DNA sequencing.
10. R.-Y. Chuang and T.-H. Chang, data not shown.
11. T. Zhong and K. T. Arndt, *Cell* **73**, 1175 (1993).
12. T. Kadowaki *et al.*, *J. Cell Biol.* **126**, 649 (1994).
13. L. Guarente, *Trends Genet.* **9**, 362 (1993).
14. S. R. Schmid and P. Linder, *Mol. Cell. Biol.* **11**, 3463 (1991).
15. P. Linder and P. P. Slonimski, *Proc. Natl. Acad. Sci. U.S.A.* **86**, 2286 (1989).
16. E. J. Strauss and C. Guthrie, *Genes Dev.* **5**, 629 (1991).
17. T. Naranda, S. E. MacMillan, J. W. B. Hershey, *J. Biol. Chem.* **269**, 32286 (1994).
18. J. de la Cruz and P. Linder, personal communication.
19. I. Hussain and M. J. Leibowitz, *Gene* **46**, 13 (1986); N. Iizuka, L. Najita, A. Franzusoff, P. Sarnow, *Mol. Cell. Biol.* **14**, 7322 (1994).
20. P. Leroy, P. Alzari, D. Sassoon, D. Wolgemuth, M. Fellous, *Cell* **57**, 549 (1989).
21. K. D. Gulyas and T. F. Donahue, *ibid.* **69**, 1031 (1992); H. Yoon, S. Miller, E. K. Pabich, T. F. Donahue, *Genes Dev.* **6**, 2463 (1992).
22. W. J. Feaver *et al.*, *Cell* **75**, 1379 (1993); J. Q. Svejstrup *et al.*, *ibid*. **80**, 21 (1995).
23. D. A. Wassarman and J. A. Steitz, *Nature* **349**, 463 (1991).
24. J. Venema and D. Tollervey, *Yeast* **11**, 1629 (1995).
25. S. L. Gee and J. G. Conboy, *Gene* **140**, 171 (1994).
26. S. B. Baim, D. F. Pietras, D. C. Eustice, F. Sherman, *Mol. Cell. Biol.* **5**, 1839 (1985).
27. Cellular Ded1p-PA protein was detected by indirect immunofluorescence microscopy [J. V. Kilmartin and A. E. Adams, *J. Cell Biol.* **98**, 922 (1984)]. Cells were grown to 1 OD_{600} unit, collected by filtration, washed extensively in 0.1 M potassium phosphate (pH 6.5), and then fixed in 0.1 M potassium phosphate (pH 6.5) buffer containing 3.7% formaldehyde for 10 min. The formaldehyde-fixed cells were digested with zymolyase 100T (Seikagaku America, Rockville, MD) for 40 min at 37°C and washed three times in a phosphate-buffered saline (PBS) solution containing 1 M sorbitol. Cells were then treated with methanol (6 min) and acetone (30 s) at –20°C and resuspended in PBL [PBS, bovine serum albumin (1 mg/ml), and 100 mM lysine] to which purified normal rabbit IgG (3.5 mg/ml) was added at 1:50 dilution for staining overnight at room temperature. The next day, cells were washed three times in PBL, and the secondary antibody, Texas Red–conjugated goat antibody to rabbit IgG (Jackson Labs), was added at 1:50 dilution and incubated at room temperature for 90 min. Cells were then washed again in PBL and stained with 4′,6-diamino-2-phenylindole (DAPI) (0.5 μg/ml). Cells were applied to slides with an equal volume of Citifluor (Marivac, Halifax, Nova Scotia, Canada) and visualized with a Zeiss Axiophot microscope with Normarski optics. Texas Red and ultraviolet filters were used to detect Texas Red– and DAPI-stained images, respectively.
28. T.-H. Chang, unpublished data.
29. We thank K. Arndt, A. Hinnebusch, P. Linder, P. Sarnow, K. Struhl, and D. Wolgemuth for plasmids and strains; Y. Liu and A. Tartakoff for performing the in situ hybridization experiments; M. Leibowitz for advice on yeast translation extracts; K. Arndt, T. Donahue, J. Hershey, A. Hinnebusch, K. Madura, W. Merrick, A. Sachs, N. Sonenberg, and J. Woolford for helpful discussions; and J. Abelson for support. Supported by funds from Ohio State University, NIH grant GM48752, and an American Cancer Society (Ohio Division) grant (T.-H.C.).

8 November 1996; accepted 27 January 1997

Structure of a Protein Photocycle Intermediate by Millisecond Time–Resolved Crystallography

Ulrich K. Genick,*† Gloria E. O. Borgstahl,*†‡ Kingman Ng,†§ Zhong Ren,† Claude Pradervand, Patrick M. Burke,‖ Vukica Šrajer, Tsu-Yi Teng, Wilfried Schildkamp, Duncan E. McRee, Keith Moffat, Elizabeth D. Getzoff

The blue-light photoreceptor photoactive yellow protein (PYP) undergoes a self-contained light cycle. The atomic structure of the bleached signaling intermediate in the light cycle of PYP was determined by millisecond time–resolved, multiwavelength Laue crystallography and simultaneous optical spectroscopy. Light-induced trans-to-cis isomerization of the 4-hydroxycinnamyl chromophore and coupled protein rearrangements produce a new set of active-site hydrogen bonds. An arginine gateway opens, allowing solvent exposure and protonation of the chromophore's phenolic oxygen. Resulting changes in shape, hydrogen bonding, and electrostatic potential at the protein surface form a likely basis for signal transduction. The structural results suggest a general framework for the interpretation of protein photocycles.

Photoreceptors link light to life. Yet, understanding the molecular mechanisms for light-induced signal transduction has been limited by difficulties in obtaining and stabilizing light-activated conformations of suitable protein samples long enough for conventional structural studies by nuclear magnetic resonance or x-ray diffraction. Thus, three-dimensional structures known for photoactive proteins (*1*, *2*) all describe proteins in their dark-state conformations. Here we present the structure of the light-activated, long-lived intermediate (I_2) in the photocycle of PYP, as determined by time-resolved, multiwavelength Laue x-ray diffraction at a spatial resolution of 1.9 Å and a time resolution of 10 ms. This structure is expected to be the biologically important signaling state.

PYP is the 125-residue, 14-kD cytosolic photoreceptor (*3*, *4*) proposed to mediate negative phototaxis (*5*) in the phototrophic bacterium *Ectothiorhodospira halophila*. The photocycle kinetics in PYP crystals (*6*, *7*) resemble those in solution (*4*, *8*). After photon absorption (wavelength of maximum absorbance λ_{max} ~446 nm), ground-state PYP (P) converts rapidly ($\ll$10 ns) to a red-shifted intermediate (I_1), then quickly ($k \approx 1 \times 10^4\ s^{-1}$) to a bleached, blue-shifted intermediate (I_2). Spontaneous return of I_2 to P by a relatively slow process ($k \approx 2$ to 3 s^{-1}) completes the photocycle. One proton is taken up by PYP during formation of I_2 and released upon return to P (*9*). The 4-hydroxycinnamyl chromophore (Fig. 1A), covalently attached to Cys^{69} through a thioester linkage, is proposed to photoisomerize during the photocycle (*10*, *11*). In the ground- or dark-state structure of PYP determined at 1.4 Å resolution (*2*), the yellow, anionic chromophore (*10*, *12*) forms a hydrogen bond with a buried glutamic acid within a hydrophobic core, protected from solvent.

The short lifetime of the I_2 intermediate and the need to simultaneously record optical data presented challenges beyond those encountered in previous Laue crystallographic studies (*13*). Specific features of our experimental system and techniques

U. K. Genick, G. E. O. Borgstahl, P. M. Burke, D. E. McRee, E. D. Getzoff, Department of Molecular Biology, Scripps Research Institute, 10550 North Torrey Pines Road, La Jolla, CA 92037, USA.
K. Ng, Z. Ren, C. Pradervand, V. Šrajer, T.-Y. Teng, W. Schildkamp, K. Moffat, Department of Biochemistry and Molecular Biology, University of Chicago, 920 East 58th Street, Chicago, IL 60637, USA.

*These authors contributed equally to this work.
†These authors made major contributions to time-resolved studies on photoactive yellow protein.
‡Present address: University of Toledo, Department of Chemistry, Toledo, OH 43606, USA.
§Present address: Eli Lilly and Company, Lilly Corporate Center, Indianapolis, IN 46285, USA.
‖Present address: Department of Pathology, University of Utah School of Medicine, Salt Lake City, UT 84132, USA.

contributed to the success of this study (*14*). PYP crystals diffract strongly, have low mosaic spread, allow repeated laser-triggering of the photocycle, and are relatively resistant to radiation damage. However, to avoid degradation of crystalline order and interference with optical measurements during continuous laser illumination, we collected data with the laser off during the decay from a saturated photostationary state established by off-peak laser illumination (*14*). The exciting laser, microspectrophotometer (*15*), and x-ray shutters (*16*) were synchronized (*7, 17*) for coordinated optical and diffraction data collection, and multiple exposures increased diffraction intensities (*14*).

Structural changes in PYP after light activation were localized near the chromophore (Fig. 1) in difference electron density maps produced from independent diffraction data processing by two methods (*18*). The data set collected 2 to 12 ms after laser shut off and processed with LaueView (*19*) provided optimal merging and wavelength scaling statistics (Table 1). Both high resolution and deconvolution of energy overlaps contributed to map quality, as assessed by comparison of electron density maps.

During the 2- to 12-ms time point in the decay from the photostationary state, ~50% of PYP molecules exhibited significant active-site structural differences from the ground state (Fig. 2), including isomerization of the chromophore. This photostationary-state structure was refined independently by conventional all-atom crystallographic refinement and by selected-atom refinement with extrapolated structure factor amplitudes (*20*). In all-atom refinement (*20*), a model for the bleached intermediate was fitted to difference (Fig. 2, A and B) and omit (Fig. 2, C and D) electron density maps, then dual conformations were refined by positional and occupancy refinement (Table 2). The resulting ~50% occupancy of the bleached conformer is about half of that predicted from a simple kinetic model (*4, 7, 8*), suggesting that photocycle physics (for example, back reactions) precluded a homogeneous population of bleached molecules under our experimental conditions. Alternatively, optical bleaching might not be directly coupled to structural changes ob-

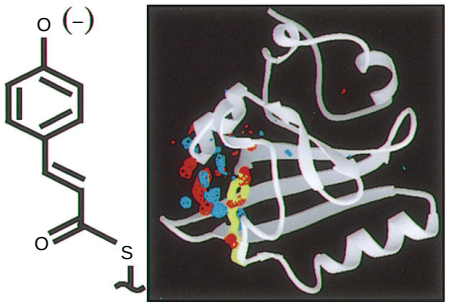

Fig. 1. Chromophore structure (**left**) and difference ($|F_{photostationary}| - |F_{dark}|$) electron density map with PYP fold in the ground state (white ribbon) and trans-chromophore (yellow) (**right**). The density map (contoured at 3σ) shows an excellent signal-to-noise ratio for the transient, light-induced, structural changes. The largest signal is localized at the active site (blue, positive; and red, negative electron density). Figures 1 to 4 were made with AVS (*28*).

Table 1. Laue x-ray diffraction data. Cum., cumulative.

	Dark state		Photostationary state	
Images (*n*)	25		24	
Reflections				
Total (*n*)	64,367		56,947	
Unique (*n*)	10,552		10,354	
R_{sym}* (%)				
Unweighted	11.8		12.5	
Weighted	8.8		9.4	
	Completeness (%)			
	Shell	Cum.	Shell	Cum.
Resolution (Å)				
10–3.0	94.2		94.9	
3.0–2.4	95.4	94.8	95.2	95.0
2.4–2.1	93.4	94.5	93.2	94.4
2.1–1.9	87.3	92.7	86.0	92.3
1.9–1.72†	66.3	86.2	62.8	85.0
1.72–1.6†	34.9	76.0	32.4	74.6

*$R_{sym} = H \Sigma_i \Sigma^{nH} (w_{Hi}|F^2_{Hi} - \langle F^2_H \rangle|) / {}_H\Sigma {}_i\Sigma^{nH} w_{Hi} \times F^2_{Hi}$, where $\langle F^2_H \rangle = {}_i\Sigma^{nH} w_{Hi} \times F^2_{Hi} / {}_i\Sigma^{nH} w_{Hi}$ and $H = (h, k, l)$, $w_{Hi} = 1$ for unweighted *R* factors and $w_{Hi} = 1/\sigma^2(F^2_{Hi})$ for weighted *R* factors. †Data from 1.9 to 1.6 Å were used for energy overlap deconvolution only.

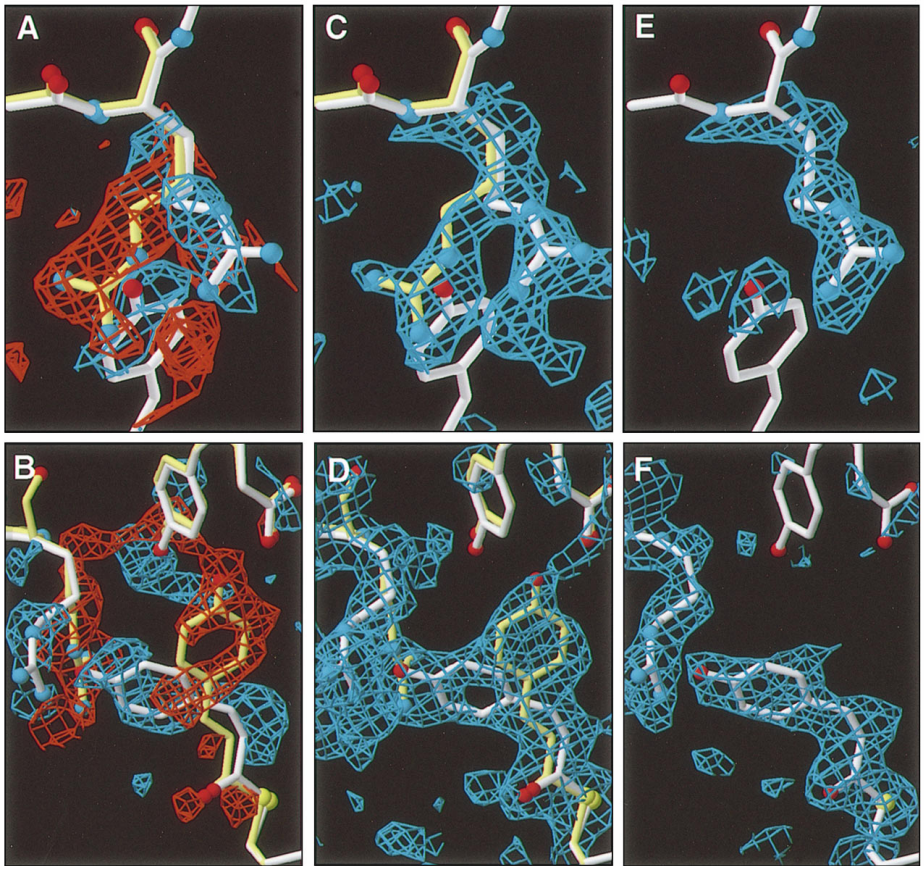

Fig. 2. Atomic positions for the bleached (white) and dark (yellow) states of PYP's active site with the three different electron density maps used for structure determination. All three show a light-induced increase in the population of the bleached state. (**Top panels**) Arg^{52} is shown above the phenolic ring of the chromophore. (**Bottom panels**) The chromophore is shown beneath Arg^{52} (left) and Tyr^{42} and Glu^{46} (above). (**A** and **B**) Difference map ($|F_{photostationary}| - |F_{dark}|$) (contoured at 2σ). Blue contours depict electron density that appears in the photostationary state; red contours depict diminished electron density. The ball of electron density (red) near Arg^{52} (A) is due to the movement of a water molecule (not shown) upon photobleaching. (**C** and **D**) Simulated-annealing omit map ($|F_{photostationary}| - |F_{calculated}|$) calculated for a model in which Arg^{52} and the chromophore were omitted (contoured at 1σ). The ratio of dark-state and bleached-state structures in the experimentally achieved photostationary state is approximately 1 to 1. (**E** and **F**) Extrapolated, simulated-annealing omit map corresponding to 100% population of the bleached structure (*20*) calculated with phases from the dark-state model in which Arg^{52} and the chromophore were omitted (contoured at 1.5σ).

servable by x-ray diffraction (*7*). In selected-atom refinement (*20*), 50% occupancies were used to extrapolate structure factor amplitudes for a hypothetical fully bleached crystal, and the bleached conformer was refined (Fig. 2, E and F). These diffraction amplitudes were in turn used for simulated annealing refinement (Table 2) in which only active-site residues associated with peaks in electron density difference maps (Fig. 2, A and B) were allowed to move. These two refinements of the bleached conformer of PYP showed light-induced structural changes that were identical within experimental error.

In the bleached structure of PYP denoted I_2, the 4-hydroxycinnamyl chromophore has undergone a light-induced trans-to-cis isomerization around the carbon-carbon double bond that is conjugated with, and located between, the phenolic ring and the thioester linkage to Cys^{69} (Fig. 3). In the photobleached cis-chromophore, collision of the thioester carbonyl with the nearest aromatic ring proton produces a strained nonplanar conformation (by ~60°) that could provide the driving force for return to the dark-state trans-isomer. In the bleached structure, the chromophore's aromatic ring has moved toward the protein surface, so that its phenolic oxygen atom is centered in the dark-state position of the Arg^{52} guanidinium group (Fig. 2, B and D). Arg^{52} has moved and reannealed to the protein surface in a new position. Consequently, the phenolic oxygen atom of the cis-chromophore becomes solvent-exposed and protonated, accounting for the proton uptake measured during formation of I_2 (*9*). Residues 42 and 45 to 51, which were neighbors of the trans-chromophore, have moved inward to partially fill the cavity left behind by the movement of the chromophore. The hydrogen bonding network that stabilized the chromophore and Arg^{52} in the dark-state structure (*2*) has undergone major rearrangement. A single hydrogen bond to the phenolic oxygen of the chromophore from Arg^{52} (Fig. 3A) has replaced the two dark-state hydrogen bonds from Glu^{46} and Tyr^{42} (Fig. 3B). These changes affect the properties of the active-site surface (Fig. 4). Arg^{52} becomes more solvent-exposed (by ~10 Å^2) and forms only a single intramolecular hydrogen bond (Fig. 3A), leaving two side-chain hydrogen donors available for interactions with other molecules. In combination with chromophore protonation, these structural rearrangements produce a patch of positive electrostatic potential (Fig. 4C). These changes in surface shape, electrostatic potential, and chemical complementarity could alter interactions of PYP with an unknown second molecule to trigger a signal transduction cascade that ultimately reverses the flagellar motor to produce negative phototaxis.

In the bleached PYP structure, the protein remains well ordered, has undergone conformational rearrangements beyond those required to avoid interatomic collisions with the isomerized chromophore, and has formed a new set of active-site hydrogen bonds, distinct from those in the dark state. These structural features are characteristic of a protein at an energy minimum, rather than in a state of acute, steric perturbation. On the basis of the structure of I_2 and photocycle kinetics of PYP (*4*, *7*, *8*), we propose a simple, structural model for the PYP photocycle. Photon absorption by the protein-bound chromophore transforms the dark or ground state (P) into the electronically excited state P* and rapidly leads to trans-to-cis isomerization of the chromophore to form the early intermediate I_1.

Table 2. Crystallographic refinement of photostationary state structure. Refl., reflections; Compl. completeness; conf., conformations.

	All-atom refinement	Selected-atom refinement	Refl.$_{F > 3\sigma}$ (n)	Compl. (%)
Refined atom positions (n)	1158	85		
Residues in molecule (n)	125	125		
Residues with dual conf. (n)	12	11		
Water molecules (n)	55	56		
Root mean square deviation				
Bond length (Å)	0.013	0.013		
Bond angles (degrees)	1.785	1.605		
R_{cryst}* (%) by resolution (Å)				
10–3.0	19.3	23.1	1975	94.4
3.0–2.4 (10–2.4)	20.3 (19.7)	23.4 (23.2)	1891 (3866)	93.9 (94.1)
2.4–2.1 (10–2.1)	20.6 (19.9)	23.6 (23.3)	1839 (5705)	90.3 (92.9)
2.1–1.9 (10–1.9)	20.3 (20.4)	26.4 (23.8)	1687 (7392)	78.4 (89.3)

*$R_{cryst} = {}_H\Sigma||F_{obs(H)}| - k|F_{calc(H)}||/{}_H\Sigma F_{obs(H)}$, standard crystallographic R factor where $F_{obs(H)}$ and $F_{calc(H)}$ are the observed and calculated structure factor amplitudes of a reflection with the indices $H = (h, k, l)$.

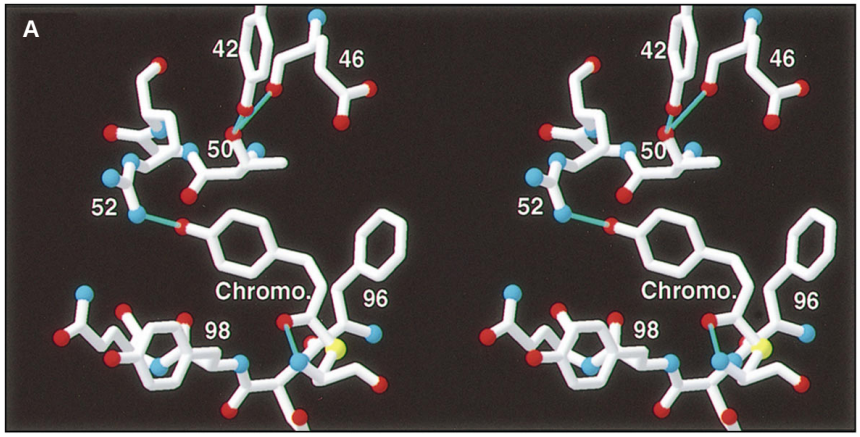

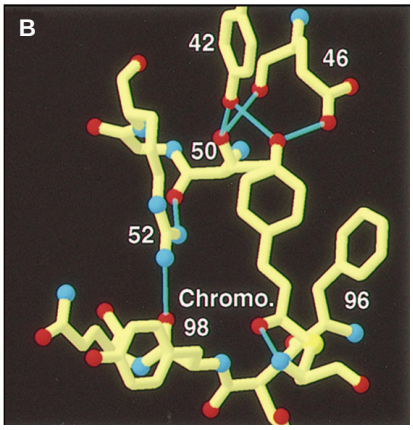

Fig. 3. Active-site hydrogen bonding networks for bleached (**A**) and dark (**B**) conformations. Oxygen (red), nitrogen (blue), and sulfur (yellow) atoms are shown as balls, and hydrogen bonds as turquoise tubes. During bleaching, dark-state hydrogen bonds from the Tyr^{42} and Glu^{46} side chains to the trans-chromophore's deprotonated phenolic oxygen (top), and from the Arg^{52} guanidinium group to the carbonyl oxygen atoms of Tyr^{98} and Thr^{50} (left), are broken. The protonated phenolic oxygen of the cis-chromophore now forms a hydrogen bond to Arg^{52} (left). Hydrogen bonds of the Cys^{69} main-chain NH with the chromophore's carbonyl group (bottom), and of the Thr^{50} side-chain OH with the Tyr^{42} side-chain OH and the Glu^{46} main-chain carbonyl oxygen (top), are conserved. The bleached-state conformation of Arg^{52} can also be fitted and refined in a flipped orientation within the same planar electron density (Fig. 2), but the location of the guanidinium group and the hydrogen bond with the cis-chromophore are conserved.

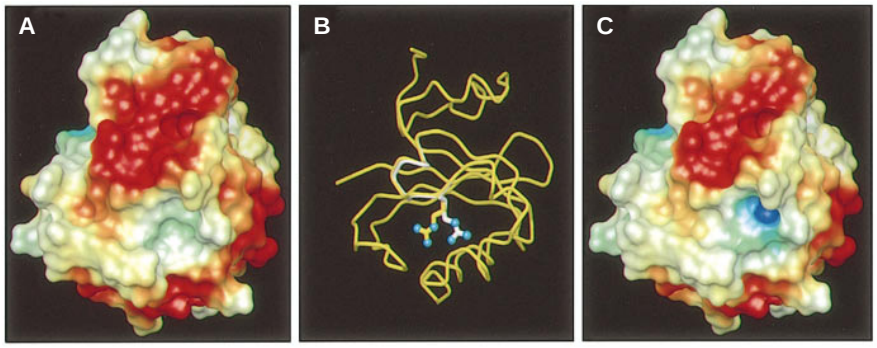

Fig. 4. Solvent-accessible molecular surface of PYP in (**A**) the dark state and (**C**) bleached state color-coded for electrostatic potential as calculated by *DelPhi* (*29*) (deep red, <-4 kT; white, neutral; dark blue, >4 kT). Partial charges were assigned according to a revised version of the CHARMM force field (*30*). In (**B**), C_α traces and side chains of Arg^{52} for the dark (yellow) and bleached (white) states are shown. Bleaching increases the positive electrostatic potential at the active site. Movements of Arg^{52} and the chromophore change the surface shape.

The extreme speed of the equivalent reaction in rhodopsin and bacteriorhodopsin (*21*) suggests that the P*-to-I_1 transition in PYP is too fast to allow substantial rearrangement of the protein. Thus, the I_1 structure would combine cis-chromophore geometry with a ground-state protein conformation. The chromophore isomerization would then trigger protein structural changes to achieve a new energy minimum, denoted I_2. After cis-to-trans chromophore reisomerization driven by physical strain in the nonplanar cis-conformation, the protein will again rearrange to the dark-state energy minimum (P), completing the photocycle. Therefore, in our model, the PYP photocycle divides into two similar halves, each characterized by fast generation of new chromophore geometry followed by slower protein rearrangement to achieve a local energy minimum. The more complex photocycles of other light-activated proteins such as rhodopsin and bacteriorhodopsin can be described as extensions of this model with additional intermediates during the protein rearrangement steps. Thus, the bleached structure and associated photocycle model for PYP provide not only the structure of a prototypical intermediate in protein-mediated signaling, but also an exemplary framework for understanding the structural mechanisms of protein photocycles.

Note added in proof: Further information about the function of Glu^{46} and Arg^{52} has recently been obtained by time-resolved spectroscopy on site-directed PYP mutants (*31*).

REFERENCES AND NOTES

1. J. Deisenhofer, O. Epp, K. Miki, R. Huber, H. Michel, *J. Mol. Biol.* **180**, 385 (1984); R. Henderson *et al.*, *ibid.* **213**, 899 (1990); G. F. X. Schertler, C. Villa, R. Henderson, *Nature* **362**, 770 (1993); W. Kuhlbrandt, D. G. Wang, Y. Fujiyoshi, *ibid.* **367**, 614 (1994); H.-W. Park, S.-T. Kim, A. Sancar, J. Deisenhofer, *Science* **268**, 1866 (1995).
2. G. E. O. Borgstahl, D. R. Williams, E. D. Getzoff, *Biochemistry* **34**, 6278 (1995).
3. T. E. Meyer, *Biochim. Biophys. Acta* **806**, 175 (1985).
4. _____, E. Yakali, M. A. Cusanovich, G. Tollin, *Biochemistry* **26**, 418 (1987); T. E. Meyer, G. Tollin, J. H. Hazzard, M. A. Cusanovich, *Biophys. J.* **56**, 559 (1989).
5. W. W. Sprenger, W. D. Hoff, J. P. Armitage, K. J. Hellingwerf, *J. Bacteriol.* **175**, 3096 (1993).
6. D. E. McRee, T. E. Meyer, M. A. Cusanovich, H. E. Parge, E. D. Getzoff, *J. Biol. Chem.* **261**, 13850 (1986).
7. K. Ng, E. D. Getzoff, K. Moffat, *Biochemistry* **34**, 879 (1995).
8. T. E. Meyer, G. Tollin, T. P. Causgrove, P. Cheng, R. E. Blankenship, *Biophys. J.* **59**, 988 (1991); W. D. Hoff *et al.*, *ibid.* **67**, 1691 (1994).
9. T. E. Meyer, M. A. Cusanovich, G. Tollin, *Arch. Biochem. Biophys.* **306**, 515 (1993).
10. M. Baca *et al.*, *Biochemistry* **33**, 14369 (1994).
11. W. D. Hoff *et al.*, *ibid.*, p. 13960; R. Kort *et al.*, *FEBS Lett.* **382**, 73 (1996).
12. M. Kim, R. A. Mathies, W. D. Hoff, K. J. Hellingwerf, *Biochemistry* **34**, 12669 (1995).
13. J. Hajdu *et al.*, *EMBO J.* **6**, 539 (1987); I. Schlichting *et al.*, *Nature* **345**, 309 (1990); B. L. Stoddard *et al.*, *Proc. Natl. Acad. Sci. U.S.A.* **88**, (1991); P. T. Singer, A. Smalas, R. P. Carty, W. F. Mangel, R. M. Sweet, *Science* **259**, 669 (1993); E. M. H. Duke, S. Wakatsuki, A. Hadfield, L. N. Johnson, *Protein Sci.* **3**, 1178 (1994); V. Fülöp *et al.*, *Structure* **2**, 201 (1994); J. M. Bolduc *et al.*, *Science* **268**, 1312 (1995).
14. PYP crystals (spacegroup $P6_3$) (*2, 6*) have high optical density that prohibits accurate optical monitoring of crystals >50 to 60 μm thick. Therefore, crystal growth was stopped at this size by transfer to a proteinless solution of 80% ammonium sulfate, 20 mM Hepes (pH 7.0; overall pH ~4.8). To reduce the effect of crystal anisotropy (*7*) on laser initiation and optical monitoring, and to exploit the crystalline symmetry for efficient diffraction data collection, we mounted crystals in capillaries with their long (~500 μm) sixfold axis roughly perpendicular to both the x-ray and optical monitoring beams. A ~5° to 10° tilt from the spindle axis allowed many symmetry-equivalent reflections to be stimulated by x-rays of different wavelength on a single image, increasing the accuracy of wavelength scaling [J. W. Campbell, J. Habash, J. R. Helliwell, K. Moffat, *Inf. Q. Protein Crystallogr.* **18**, 23 (1986)]. The 1-mm-diameter beam of the stimulating continuous-wave argon ion laser (Coherent) was unpolarized to further minimize the effects of optical anisotropy. The power and duration of laser illumination at 496.5 nm were the minimum values (100 mW/mm^2 for 200 ms) needed to produce a plateau in crystal bleaching. This wavelength, in the tail of PYP's absorption peak, allowed effective crystal penetration, thus minimizing thermal artifacts (*15, 22*). After laser shutoff, optical difference spectra were continuously recorded with a single-crystal microspectrophotometer (*15*) in the 380- to 520-nm range (*7*). After a variable delay period (2 ms in the reported experiment), a magnetic "alligator" solenoid shutter (*16*) opened and exposed the crystal to a 10-ms, polychromatic x-ray pulse from the National Synchrotron Light Source (NSLS) beamline X-26C at Brookhaven National Laboratory (*23*) (300-μm collimator, 200-mm crystal-to-detector distance, 150-μm aluminum filter). After a 30-s period for recovery from transient irradiation effects, the experiment was repeated. Ten to 16 exposures were collected on a single image plate (Fuji), before rotation of the crystal to a new spindle position (4° offset). Crystals were cooled to −12°C (FTS cooling device) to slow down the photocycle. As a control, we collected dark-state diffraction data by repeating the same procedure without laser illumination.
15. Y. Chen, V. Šrajer, K. Ng, A. D. LeGrand, K. Moffat, *Rev. Sci. Instrum.* **65**, 1506 (1994).
16. D. Bourgeois *et al.*, *J. Synchrotron Rad.* **3**, 65 (1996).
17. K. Moffat, Y. Chen, K. Ng, D. McRee, E. D. Getzoff, *Philos. Trans. R. Soc. London Ser. A* **340**, 175 (1992).
18. LaueView (*19*) processing of the 2- to 12-ms data set to 1.6 Å resolution included deconvolution of spatially and energy-overlapped spots. Therefore, the data sets were complete even at low resolution. Additionally, the choice of wavelength range (0.7 to 2.0 Å) and data collection at many orientations increased the likelihood that almost every reflection was observed as a singlet in at least one crystal orientation. From ∞ to 3.2 Å ($2d_{min}$) resolution, the inclusion of deconvoluted reflections almost doubled the PYP data redundancy and increased the completeness from 84.7 to 93.9%. Even in the lowest shells (∞ to 4.8 Å), the quality of harmonically overlapped reflections (R_{scale} = 7.0%) was comparable to that of single reflections (R_{scale} = 6.5%). $R_{scale} = \Sigma_H |F_H^{mono} - F_H^{Laue}| / \Sigma_H |F_H^{mono} + F_H^{Laue}|$, where H represents the h, k, l indices and F_H^{mono} the structure factors from the monochromatic structure determination. Merging R factors between dark-state and photostationary-state data sets (*19*) show poor signal-to-noise ratios beyond 1.9 Å resolution, so only data to 1.9 Å were used for structure determination. As a control, data were processed with the Daresbury Laue suite of programs (*24*). Anisotropically streaked profiles were used for spatial overlap prediction and integration of ~45,000 reflections per data set in the wavelength range 0.65 to 1.65 Å. Merging of diffraction data by AGROVATA and ROTAVATA [The CCP4 Suite: Programs for Protein Crystallography, *Acta Crystallogr.* **D50**, 760 (1994)] gave unweighted merging R factors for native and bleached data sets of 18.9 and 21.2%, respectively. Data were >76% complete overall (12.0 to 2.0 Å) and >57% complete in the highest resolution shell (2.08 to 2.0 Å).
19. Z. Ren and K. Moffat, *J. Synchrotron Rad.* **1**, 78 (1994); *J. Appl. Crystallogr.* **28**, 461 (1995); *ibid.*, p. 482; Z. Ren, K. Ng, G. E. O. Borgstahl, E. D. Getzoff, K. Moffat, *ibid.* **29**, 246 (1996).
20. For the all-atom approach, PYP dark-state atomic coordinates (*2*) without the chromophore, Arg^{52} side chain, and all water molecules were positionally refined with XPLOR (*25*) against photostationary-state data between 10 and 1.9 Å with $I/\sigma I > 3$ (starting R factor 29.6%). Alternative conformations for the chromophore and residues 42, 45 to 52, 62, and 124 in the bleached structure were fit with XtalView (*26*) to difference ($|F_{photostationary}| - |F_{dark}|$) (Fig. 2, A and B) and omit (Fig. 2, C and D) electron density maps. Further positional, B factor, and occupancy refinement gave an overall R factor of 20.4%. Relative occupancies of the two conformers were determined to be 0.5 each by examination of $|F_{obs}| - |F_{calc}|$ electron density maps and occupancy refinement of nonoverlapping atoms (four chromophore ring atoms and Arg^{52} C_δ and N_ϵ). For the selected-atom approach, the 10 bleached-state residues (chromophore and active-site residues 42 and 45 to 52) associated with strong peaks in the $|F_{photostationary}| - |F_{dark}|$ electron density map (Fig. 1) were refined against $|F_{extrapolated}|$. All other residues were fixed to the coordinates of the monochro-

matic dark-state structure (*2*). $|F_{extrapolated}|$ values were calculated by linear extrapolation from $|F_{dark}|$ and $|F_{photostationary}|$, by assuming equal occupancies of dark and bleached conformers in the photostationary state $|F_{extrapolated}| = 2 \times (|F_{photostationary}| - |F_{dark}|) + |F_{dark}|$. To enable structural changes and reduce model bias, we used the slowcool simulated annealing protocol in XPLOR with a 10-fold increased weighting ratio (W_A) (*25*) between x-ray and stereochemical terms. The resulting coordinates of the 10 selected residues were combined with monochromatic dark-state coordinates, as alternative conformers representing the bleached structural state. Positional and *B*-factor refinement of the combined coordinates against $|F_{photostationary}|$, again restricting movement to the 10 selected residues of the bleached structure, gave an *R* factor of 23.8%. The higher *R* factor of the selected-atom refinement is due to structural changes away from the active site that reflect systematic errors or changes in experimental conditions between the monochromatic (*2*) and Laue data sets. Those changes were also observed in refinement of dark-state coordinates against dark-state Laue data (*R* factor 20.7%) (*27*). Therefore, compared to the previously published dark-state structure (*2*), coordinates from the selected-atom refinement better indicate changes due solely to photobleaching and were used for all figures.

21. R. A. Mathies, S. W. Lin, J. B. Ames, W. T. Pollard, *Annu. Rev. Biophys. Biophys. Chem.* **20**, 491 (1991); Q. Wang, R. W. Schoenlein, L. A. Peteneau, R. A. Mathies, C. V. Shank, *Science* **266**, 422 (1994).
22. D. W. J. Cruickshank, J. R. Helliwell, L. N. Johnson, *Philos. Trans. R. Soc. London* **340**, 167 (1992).
23. E. D. Getzoff *et al*., *Nucl. Instrum. Methods Phys. Res.* **79**, 249 (1994).
24. J. R. Helliwell *et al*., *J. Appl. Crystallogr.* **22**, 483 (1989); T. J. Greenhough and A. K. Shrive, *ibid.* **27**, 111 (1994); J. W. Campbell, *ibid.* **28**, 228 (1995).
25. A. T. Brünger, J. Kuriyan, M. Karplus, *Science* **235**, 458 (1987); A. T. Brünger, A. Krukowski, J. W. Erickson, *Acta Crystallogr. A* **46**, 585 (1990).
26. D. E. McRee, *J. Mol. Graph.* **10**, 44 (1992); D. E. McRee, *Practical Protein Crystallography* (Academic Press, San Diego, CA, 1993).
27. U. K. Genick *et al*., unpublished data.
28. C. Upson *et al*., *IEEE Comput. Graph. Appl.* **9**, 30 (1989).
29. A. Nicholls and B. Honig, *J. Comput. Chem.* **12**, 435 (1991); A. Nicholls, K. A. Sharp, B. Honig, *DelPhi* (Department of Biochemistry and Molecular Biophysics, Columbia University, New York, NY, 1990).
30. A. D. MacKerell *et al*., *FASEB J.* **6**, A143 (1992); A. D. MacKerell Jr. *et al*., in preparation.
31. U. K. Genick *et al*., *Biochemistry* **36**, 8 (1997).
32. We thank E. Blum, Y. Chen, A. LeGrand, H. E. Parge, and G. Shea-McCarthy for assistance in designing and constructing apparatus for these experiments and for help with data collection at NSLS, Brookhaven National Laboratory, and previous runs at CHESS, Cornell University; T. Greenhough for help with the Daresbury Laue program suite; J. A. Tainer and M. Baca for valuable discussions; and M. E. Pique for help with AVS figures. Coordinates for the PYP bleached intermediate have been deposited in the Protein Data Bank (accession number 2pyp). Supported by grants from NIH (GM37684 to E.D.G.; GM36452 and RR07707 to K.M.) and the W. M. Keck Foundation (M. Makinen and K.M.), and fellowships from NIH (NRSA GM15820 to G.E.O.B.) and Boehringer Ingelheim Fonds (U.K.G.).

26 June 1996; accepted 26 December 1996

PTG, a Protein Phosphatase 1–Binding Protein with a Role in Glycogen Metabolism

John A. Printen,* Matthew J. Brady,* Alan R. Saltiel†

Protein dephosphorylation by phosphatase PP1 plays a central role in mediating the effects of insulin on glucose and lipid metabolism. A PP1C-targeting protein expressed in 3T3-L1 adipocytes (called PTG, for protein targeting to glycogen) was cloned and characterized. PTG was expressed predominantly in insulin-sensitive tissues. In addition to binding and localizing PP1C to glycogen, PTG formed complexes with phosphorylase kinase, phosphorylase a, and glycogen synthase, the primary enzymes involved in the hormonal regulation of glycogen metabolism. Overexpression of PTG markedly increased basal and insulin-stimulated glycogen synthesis in Chinese hamster ovary cells overexpressing the insulin receptor, which do not express endogenous PTG. These results suggest that PTG is critical for glycogen metabolism, possibly functioning as a molecular scaffold.

The critical role of protein phosphorylation in the regulation of glucose and lipid metabolism has been recognized since the pioneering work of Krebs and Fischer in the 1950s (*1*). Insulin modulates many of the metabolic rate–limiting enzymes by promoting their net dephosphorylation, due to the activation of the type 1 serine-threonine protein phosphatase 1 (PP1) (*2*). Although the signaling pathways linking the insulin receptor to PP1 activation remain uncertain (*3*), the catalytic subunit of PP1 (PP1C) is thought to be maintained at discrete cellular locations in order to ensure the specificity of protein dephosphorylation produced by insulin (*4*). In mammals, two tissue-specific proteins have been identified that target PP1C to glycogen. RG1 encodes a protein product of 124 kD that is present in both heart and skeletal muscle (*5*). GL encodes a 33-kD glycogen and PP1C-binding subunit expressed exclusively in liver (*6*). Although phosphorylation of RG1 by the mitogen-activated protein kinase pathway was implicated in the regulation of PP1 activity (*7*), numerous studies have demonstrated that this phosphorylation cascade is neither necessary nor sufficient for the regulation of glycogen synthesis by insulin (*8*, *9*).

We used 3T3-L1 adipocytes, which are highly responsive to insulin, to identify PP1C-binding proteins that might be involved in insulin-mediated regulation of glycogen metabolism. A 3T3-L1 adipocyte cDNA library (*10*) fused to the Gal4p transcriptional activation domain was screened for proteins that interact with a Gal4p-PP1C DNA-binding domain fusion (*11*). Library plasmids expressing interacting proteins were identified by the ability to induce transcription of the integrated GAL1-lacZ reporter. One class of interacting cDNAs, typified by clone B1-1, consistently gave the highest levels of β-galactosidase (β-Gal) activity when plated on X-Gal–containing media. Partial DNA sequence from the GAL4 fusion junction followed by a BLAST search revealed that the cDNA contained in clone B1-1 was homologous to previously cloned PP1C glycogen-localizing subunits. Sequencing of an additional clone (B2-2) from the same class provided a probable translational initiation site (*12*). The PP1C-interacting cDNA contained in clones B1-1 and B2-2 was named PTG (protein targeting to glycogen).

PTG has amino acid sequence similarity to known glycogen-binding subunits of PP1C (Fig. 1). PTG is most similar to G_L (42% identity, 60% similarity), with less similarity to the skeletal muscle protein RG1 (26% identity, 49% similarity) and the yeast glycogen-binding subunit Gac1 (27% identity, 50% similarity) (*13*). The phosphorylation sites in RG1 that have been implicated in hormonal control of PP1C activity (*7*) are not conserved in PTG.

Northern (RNA) analysis of rat tissue revealed a PTG transcript of 3.0 kb expressed in all tissues except testis, being most abundant in skeletal muscle, liver, and heart. The 3.0-kb PTG transcript was also detected when 3T3-L1 fibroblasts were induced to differentiate into adipocytes (*14*), a transition correlated with a substantial increase in insulin sensitivity, including the stimulation of glycogen synthesis (*15*).

To determine whether PTG binds simultaneously to PP1C and glycogen, we evaluated their association in intact cells. A FLAG epitope–tagged PTG construct (pF-PTG) (*16*) was transiently transfected into Chinese hamster ovary cells overexpressing the insulin receptor (CHO-IR) (*17*), followed by immunoprecipitation with antibodies to FLAG (anti-FLAG) (*18*) and sub-

J. A. Printen and A. R. Saltiel, Department of Physiology, University of Michigan School of Medicine, Ann Arbor, MI 48109, and Department of Cell Biology, Parke-Davis Pharmaceutical Research Division, Warner-Lambert Company, Ann Arbor, MI 48105, USA.
M. J. Brady, Department of Cell Biology, Parke-Davis Pharmaceutical Research Division, Warner-Lambert Company, Ann Arbor, MI 48105, USA.

*These authors contributed equally to this work.
†To whom correspondence should be addressed.